

First results from CSSWE CubeSat: Characteristics of relativistic electrons in the near-Earth environment during the October 2012 magnetic storms

X. Li,^{1,2} Q. Schiller,^{1,2} L. Blum,^{1,2} S. Califf,^{1,2} H. Zhao,^{1,2} W. Tu,³ D. L. Turner,⁴ D. Gerhardt,² S. Palo,² S. Kanekal,⁵ D. N. Baker,¹ J. Fennell,⁶ J. B. Blake,⁶ M. Looper,⁶ G. D. Reeves,³ and H. Spence⁷

Received 19 August 2013; revised 7 October 2013; accepted 8 October 2013.

[1] Measurements from the Relativistic Electron and Proton Telescope integrated little experiment (REPTile) on board the Colorado Student Space Weather Experiment (CSSWE) CubeSat mission, which was launched into a highly inclined (65°) low Earth orbit, are analyzed along with measurements from the Relativistic Electron and Proton Telescope (REPT) and the Magnetic Electron Ion Spectrometer (MagEIS) instruments aboard the Van Allen Probes, which are in a low inclination (10°) geo-transfer-like orbit. Both REPT and MagEIS measure the full distribution of energetic electrons as they traverse the heart of the outer radiation belt. However, due to the small equatorial loss cone (only a few degrees), it is difficult for REPT and MagEIS to directly determine which electrons will precipitate into the atmosphere, a major radiation belt loss process. REPTile, a miniaturized version of REPT, measures the fraction of the total electron population that has small enough equatorial pitch angles to reach the altitude of CSSWE, $480\text{ km} \times 780\text{ km}$, thus measuring the precipitating population as well as the trapped and quasi-trapped populations. These newly available measurements provide an unprecedented opportunity to investigate the source, loss, and energization processes that are responsible for the dynamic behavior of outer radiation belt electrons. The focus of this paper will be on the characteristics of relativistic electrons measured by REPTile during the October 2012 storms; also included are long-term measurements from the Solar Anomalous and Magnetospheric Particle Explorer to put this study into context.

Citation: Li, X., et al. (2013), First results from CSSWE CubeSat: Characteristics of relativistic electrons in the near-Earth environment during the October 2012 magnetic storms, *J. Geophys. Res. Space Physics*, **118**, doi:10.1002/2013JA019342.

1. Introduction

[2] Earth's radiation belts are usually divided into the inner belt, centered near $L=1.5$ (where L is a dimensionless parameter describing the magnetic shell that represents the geocentric distance in Earth radii (R_E) at the equator of the shell if the Earth's magnetic field is approximated as a

dipole), and the outer radiation belt that is most intense between L of 4 and 5. Earth's outer radiation belt consists of electrons in the energy range from 100 s of keV to a few MeV. Compared to the inner radiation belt, which usually contains somewhat less energetic electrons but a very intense population of protons extending in energy up to several hundreds of MeV or even GeV, the outer belt consists of energetic electrons that show a great deal of variability that is well correlated with geomagnetic storms and high-speed solar wind streams [Williams, 1966; Paulikas and Blake, 1979; Baker *et al.*, 1979, 2005].

[3] Figure 1 shows yearly window-averaged sunspot numbers and weekly window-averaged solar wind speed (km/s) in the top panel and monthly window-averaged fluxes of ~ 2 MeV electrons ($\#/cm^2\text{-s-sr}$) from Solar Anomalous and Magnetospheric Particle Explorer (SAMPEX) [Cook *et al.*, 1993] and Colorado Student Space Weather Experiment (CSSWE) [Li *et al.*, 2011b, 2012, 2013]. The period covers from SAMPEX's launch (3 July 1992, into a $550 \times 650\text{ km}$ altitude and 82° inclination orbit) to almost its reentry (13 November 2012) and extends to include CSSWE measurements (5 October 2012 to 7 March 2013) from a similar orbit. The overplotted black curve represents the monthly window-average of the *Dst* index, which indicates the onset,

¹Laboratory for Atmospheric and Space Physics, University of Colorado at Boulder, Boulder, Colorado, USA.

²Department of Aerospace Engineering Sciences, University of Colorado at Boulder, Boulder, Colorado, USA.

³Space Science and Applications, ISR-1 Los Alamos National Laboratory, Los Alamos, New Mexico, USA.

⁴Department of Earth, Planetary, and Space Sciences, University of California, Los Angeles, California, USA.

⁵NASA/GSFC, Greenbelt, Maryland, USA.

⁶Space Sciences Department of The Aerospace Corporation, Los Angeles, California, USA.

⁷Institute for the Study of Earth, Oceans and Space, University of New Hampshire, Durham, New Hampshire, USA.

Corresponding author: X. Li, Laboratory for Atmospheric and Space Physics, University of Colorado at Boulder, Boulder, CO 80303, USA.
(xinlin.li@lasp.colorado.edu)

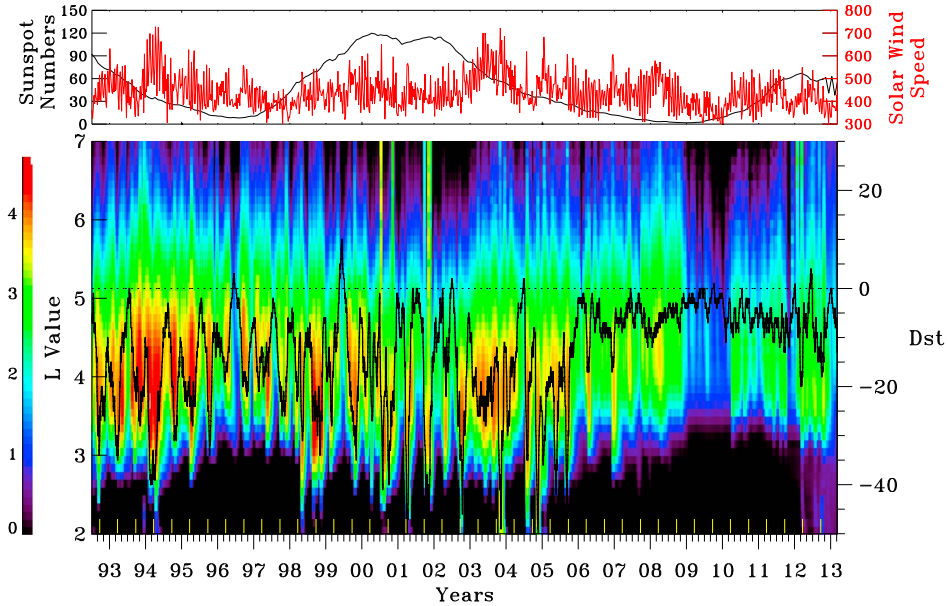


Figure 1. (top) Variations of yearly window-averaged sunspot numbers (black curve) and weekly window-averaged solar wind speed (km/s, red curve). (bottom) Monthly window-averaged, color coded in logarithm, and sorted in L (L bin: 0.1) electron fluxes of ~ 2 MeV ($\#/cm^2\text{-s-sr}$) measured by SAMPEX since its launch (3 July 1992) into a low-altitude (550×600 km) and highly inclined (82°) orbit to its reentry (13 November 2012), and CSSWE/REPTile measurements of 1.68–3.8 MeV electrons (5 October 2012 to 7 March 2013) from a similar altitude. The superimposed black curve represents monthly window-averaged Dst index. The yellow vertical bars on the horizontal axis mark the equinoxes. Calibrated daily averaged electron fluxes from SAMPEX are only available up to day 74 of 2004. We also have daily count rates from the same instrument, proton and electron telescope/electron of low energy (PET/ELO), from day 1 of 2003 to day 289 of 2009 and from a different instrument, heavy ion large telescope (HILT), throughout the mission. For the period where the flux data and count rate data overlap, we performed a linear least squares fit independently for each of the 60 L shell bins. This gave two coefficients for each L shell bin, which best convert the count rate to pseudo-flux (after day 74 of 2004). For the last few weeks of the SAMPEX mission, when its altitude dropped below 200 km, we use CSSWE/REPTile measurements to normalize the measurements.

duration, and magnitude of magnetic storms. It is evident in Figure 1 that the intensity of outer belt electrons is very well correlated with the solar wind speed. However, the essential feature required for enhancements of the MeV electron fluxes is geomagnetic activity that in turn requires a southward component of the interplanetary magnetic field (IMF) [Li *et al.*, 2011a]. The outer belt electrons exhibit a strong solar cycle and seasonal variation. The electron flux is most intense, on average, during the declining phase of the sunspot cycle (1993–1995; 2003–2005), weakest during sunspot minimum (1996–1997; 2008–2010). In particular, the outer belt electron flux was unusually low during 2008–2010 and so was the geomagnetic activity as indicated by the averaged Dst curve. The inward penetration of the MeV electrons is well correlated with the magnitude of the Dst index [Tverskaya, 1986; Zhao and Li, 2013]. Here we show the same that the trend is still evident for the monthly window-averaged electron flux and Dst index. Seasonally, the outer belt is most intense around the equinoxes [Baker *et al.*, 1999] and also penetrates the deepest around the equinoxes [Li *et al.*, 2001]. In Figure 1, equinoxes are marked by the vertical yellow bars along the horizontal axis. It is worth noting that the enhancements during the October 2012 magnetic storms, the period of interest for the rest

of this paper, are not particularly strong in terms of absolute intensity but they are among the strongest enhancements after years of dormancy.

[4] The physical mechanism for the enhancement of the outer belt electrons is under debate. One school of thought is that solar wind variations perturb the magnetosphere generating ultra low frequency (ULF) waves [Engelbreton *et al.*, 1998; Vennstrom, 1999], which drive radial diffusion [Rostoker *et al.*, 1998; Baker *et al.*, 1998; Li *et al.*, 1999; Mathie and Mann, 2000, 2001; O'Brien and Moldwin, 2003; Barker *et al.*, 2005; Ukhorskiy *et al.*, 2006; Li *et al.*, 2007; Tu *et al.*, 2009; Tu and Li, 2011; Tu *et al.*, 2012] and thus energize electrons. Magnetohydrodynamic simulations and test-particle tracing have shown that radiation belt electrons respond to such magnetospheric fluctuations [Hudson *et al.*, 1999; Elkington *et al.*, 1999; Kress *et al.*, 2007]. Recently, the paradigm for explaining the enhancement of the electron radiation belt has shifted from the almost exclusive use of the theory of radial diffusion to a greater emphasis on the role of waves in the *in situ* heating of radiation belt electrons. The waves are produced by the injection of plasma-sheet electrons into the inner magnetosphere [Horne and Thorne, 2003; Shprits *et al.*, 2006; Chen *et al.*, 2007; Kasahara *et al.*, 2009; Bortnik and Thorne, 2007; Yoon, 2011; Turner *et al.*, 2013; Reeves *et al.*, 2013]. Though it

has become generally accepted that both mechanisms can energize radiation belt electrons, their relative contributions remain uncertain.

[5] In a recent analysis of the newly available Radiation Belt Storm Probes-Energetic Particle, Composition, and Thermal Plasma [Spence *et al.*, 2013] data from Magnetic Electron Ion Spectrometer (MagEIS) [Blake *et al.*, 2013] and Relativistic Electron and Proton Telescope (REPT) [Blake *et al.*, 2013] on board the Van Allen Probes spacecraft (<http://vanallenprobes.jhuapl.edu>) [Kessel *et al.*, 2012], Reeves *et al.* [2013] conclude that the observed radial profiles of phase space density are characteristic of local acceleration in the heart of the outer radiation belt during the 8–9 October 2012 magnetic storms. Here we investigate the same storm periods but focus on the characteristics of outer radiation belt electrons in the near-Earth environment and discuss the contribution of precipitation loss to the overall outer belt variations. We show that measurements in a highly inclined low Earth orbit (LEO) are critical to determination of the precipitation loss and thus the real amount of acceleration of the outer belt electrons. Using LEO measurements from the CSSWE CubeSat, we conclude that the total enhancements during 9 October 2012 storm are likely more than what were shown in Reeves *et al.* [2013] by 12.7% for 0.58 MeV energy and 14.6% for 1.63 MeV energy electrons around the $L=4$ (the center location of phase space density peak) due to additional loss not accounted for in that work.

[6] We will first describe the CubeSat mission and its only science payload, REPTile, present REPTile measurements, and compare them with measurements from MagEIS and REPT during the period centered on the storms in early October of 2012. We will then show the populations of trapped, quasi-trapped, and untrapped electrons measured by REPTile and address the total precipitation loss, followed by discussions and conclusions.

2. CSSWE Mission and Instrument Descriptions

[7] The Colorado Student Space Weather Experiment (CSSWE: <http://lasp.colorado.edu/home/csswe/>) is a three-unit (10 cm × 10 cm × 30 cm) CubeSat mission funded by the National Science Foundation, launched into a low-altitude, highly inclined orbit on 13 September 2012 as a secondary payload under NASA's Educational Launch of Nanosatellites program [Li *et al.*, 2011b, 2012, 2013]. CSSWE contains a single science payload, the Relativistic Electron and Proton Telescope integrated little experiment (REPTile). REPTile is a miniaturization of the Relativistic Electron and Proton Telescope (REPT) [Baker *et al.*, 2012] built at the University of Colorado's Laboratory for Atmospheric and Space Physics (LASP) for the NASA/Van Allen Probes mission. REPTile is designed to measure the directional differential flux of protons ranging between 9 and 40 MeV and electrons ranging between 0.58 and >3.8 MeV. These energetic particles can have deleterious effects on the operations and lifetimes of Earth-orbiting spacecraft and astronauts during their extravehicular activity.

[8] The entire CSSWE system, including its ground station, was designed, built, calibrated, tested, delivered, and operated by students, mentored and helped along the way by professionals of LASP and others, using all commercial off the shelf parts. The commissioning phase was completed on 4 October 2012 when REPTile was turned

on. The primary mission was designed for 3 months (minimum mission for 1 month). Limited by the extreme budgets imposed on CubeSats—mass, volume, power, and data link—the CSSWE architecture follows the “keep it simple” method and the system design was always simplified to meet the requirements rather than designed to push the envelope.

[9] REPTile has a simple and robust design verified with Geometry and Tracking 4 (Geant4) simulations [Agostinelli *et al.*, 2003]. The instrument consists of four solid state detectors encased in aluminum and tungsten shielding. REPTile uses the depth of penetration of the particle into the detector stack to infer the energy of incoming particles. Particles must also have adequate energy to penetrate through a thin beryllium foil to reach the first detector [Li *et al.*, 2012], and then the particle species is determined based on the energy deposited in each detector. Particles depositing $0.25 < E < 1.5$ MeV are classified as electrons, and those depositing $E > 4.5$ MeV as protons. The particle's incident energy is determined by its penetration distance in the detector stack using coincidence binning logic. Following launch and commissioning, detector #3 in the stack had unusually low gain and was turned off. Recalibration was performed for the remaining three operational detectors. With the help of Geant4 simulations, the energy channels are determined to be: 0.58–1.63, 1.63–3.8, and >3.8 MeV for electrons and 9–18, 18–30, and 30–40 MeV for protons. The resulting channel efficiencies are shown in Figure 2. Figure 2 (left) shows the results of Geant4 simulation for one million electrons targeted down the bore sight of the instrument at energies ranging from 100 keV up to 10 MeV. Figure 2 (right) shows similar results, now for 250,000 protons at energies from 1 MeV to 50 MeV. The black line indicates particles which impact the detector corresponding to that energy channel after penetrating the beryllium foil and all “upstream” detectors, the red line shows particles binned as electrons after going through the onboard binning logic, and the blue line shows particles binned as protons. Protons can be masqueraded as electrons, as shown in Figure 2 (right). However, unless there is a significant solar energetic particle event, energetic (>10 MeV) proton fluxes in the outer belt region are very low and their effect on outer belt electron measurement is negligible.

[10] The raw, 6 s count rates received on the ground are processed to remove transmission noise by deleting data points within 12 s of a transmission event. Furthermore, during periods of high solar beta angle (the angle between the sun vector and the satellite orbital plane), the spacecraft interior temperature increased, causing an increase in the leakage current created from the biased detectors. Periods affected by this temperature-dependent noise are also removed from the data. The data are additionally processed for electronics dead time correction using Poisson counting statistics

$$\text{Counts}_{\text{Corrected}} = \frac{\text{Counts}_{\text{Raw}}}{(1 - \tau \text{Counts}_{\text{Raw}})}$$

where τ is $10\ \mu\text{s}$, the approximate response time of the electronics chain. The dead time correction peaks during very high count rates, where it takes a value of $\sim 1.8 \times \text{Counts}_{\text{raw}}$. Also during high count rate events, certain components in the instrument electronics become less efficient at counting the number of incident particles. Specifically, the baseline of the Amptek A225 charge sensitive amplifier drifts

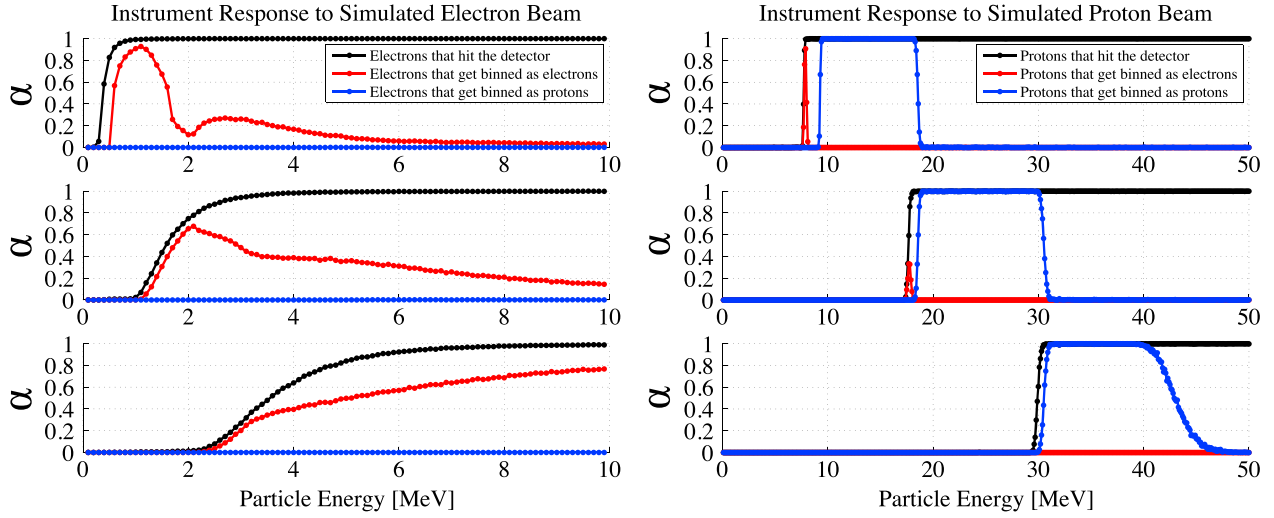


Figure 2. The response of the instrument for (left) electrons and (right) protons using Geant4. The top panels correspond to energy channel #1 (first detector), the middle to channel #2 (second detector), and the bottom to channel #3 (fourth detector). Third detector failed on launch, and these functions are the result of the recalibration.

downward with increased input pulse rate, which causes particles near the lower binning threshold to go uncounted. This effect is corrected for by characterizing the performance of the A225s to determine the lowest energy of measurable particles as a function of count rate, which increases linearly with incident count rate. Thus, with knowledge of the lower energy limit on each channel, particles that are not counted can be corrected for by assuming an energy spectrum. An $E^{-\gamma}$ spectrum, where $\gamma=2$ (determined by comparing to MagEIS medium energy spectra), is assumed for convenience, although in reality the spectrum changes as a function of time and space.

[11] The corrected counts are converted to flux as follows:

$$C_{\text{Corrected},i} = \int_0^{\infty} j \gamma \alpha_i j \gamma \alpha_i dE$$

where C stands for Counts, i corresponds to the energy channel, j the particle flux [$\#/\text{MeV}/\text{s}/\text{sr}/\text{cm}^2$], γ the geometric factor of the instrument ($0.526 \text{ [sr cm}^2]$), and α the efficiency of the channel (Figure 2). The value α represents the likelihood of an incident particle to be correctly binned by the onboard logic and is derived from particle/matter interactions simulated using Geant4 software. The instrument response for each channel is corrected to be 100% efficient over the range of the energy channel using the assumed energy spectrum. For reference, the correction factors generated from a $\gamma=4$ spectrum vary from a $\gamma=3$ spectrum by 12%, 14%, and 18% for electrons, and by 2%, 2%, and 0% for protons for the first, second, and third channels, respectively. Likewise, the correction factors generated from a $\gamma=2$ spectrum vary from the $\gamma=3$ spectrum by 12%, 14%, and 14% for electrons and by 4%, 4%, and 1% for protons. Bow-tie analysis, which convolves multiple incident flux spectra with the instrument response function to find the effective geometric factors and thresholds that are independent of spectral form [e.g., Van Allen *et al.*, 1974], would be a more accurate representation of the instruments response to incident spectra, but due to the relatively small variation

in correction for realistic spectra ($2 < \gamma < 4$), this method is sufficient for the analysis shown in this paper.

[12] The attitude control system for CSSWE is entirely passive [Li *et al.*, 2012]. A bar magnet and hysteresis rods act to roughly align the long axis of the spacecraft with the background magnetic field. The attitude with respect to Earth's magnetic field is known after analyzing the housekeeping data. Figure 3 shows the alignment of the instrument boresight for a typical 10 min period. REPTile's look direction is, for the vast majority of the time, close to 90° with

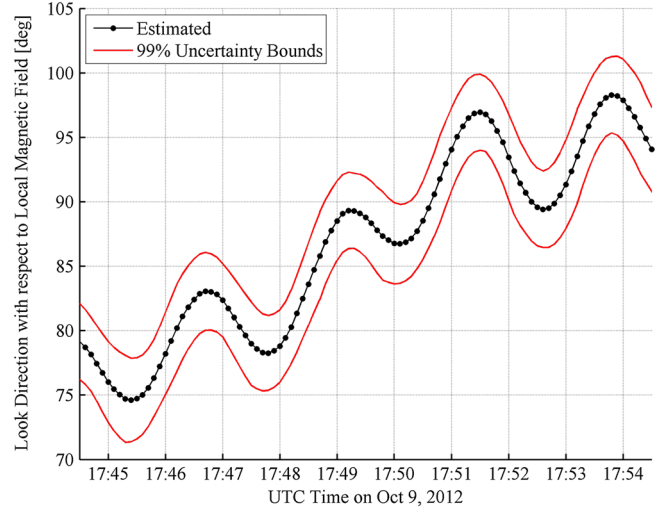


Figure 3. The look direction of the instrument with respect to Earth's local magnetic field. These 10 min are representative of attitude determination performance during isolated periods (when sun-sensing photodiodes are active). The attitude data are available every 6 s. The uncertainty bounds are calculated using a Multiplicative Extended Kalman Filter, which uses an attitude dynamics model instead of rate gyrometers. [Markley, 2003; Burton *et al.*, 2013].

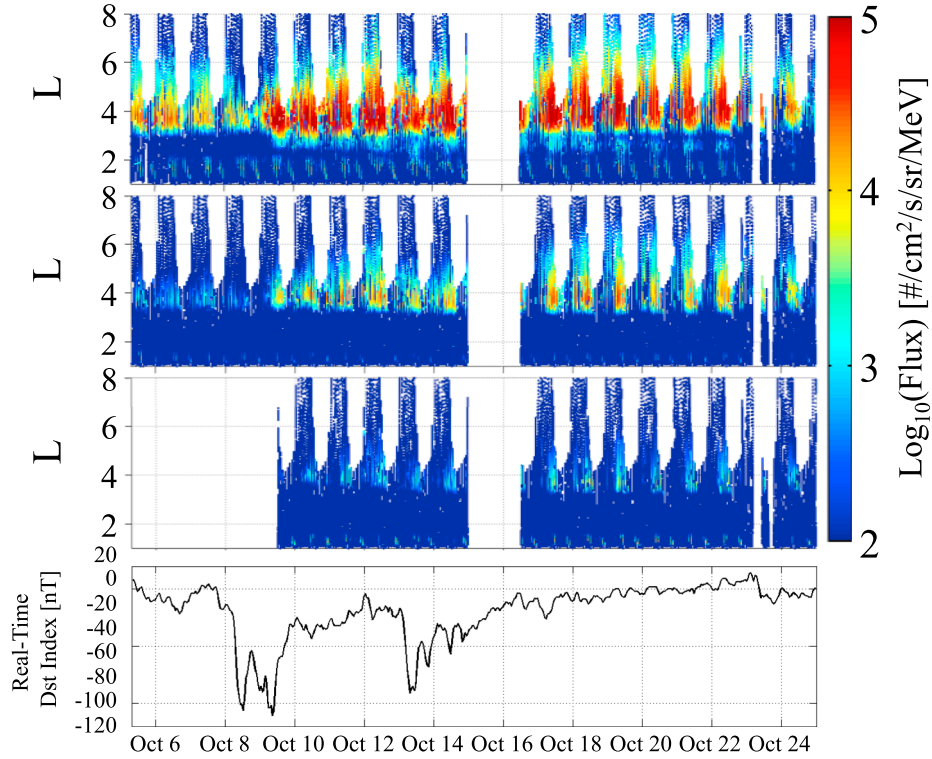


Figure 4. Electron fluxes measured by CSSWE/REPTile for the first 20 days and the Dst index. (top three panels) Color coded in logarithm and sorted in L (L bin: 0.1) electron fluxes from REPTile (every 6 s) in the energy range of 0.58–1.63, 1.63–3.8, and >3.8 MeV. (bottom) Dst index. The logic binning on channel three was activated later than the two channels. CSSWE went into safe mode during 15–16 October most likely due to a latch-up in one of the analog-to-digital converters, leading to the data gap.

respect to the background magnetic field and thus measuring locally mirroring particles. However, as the field of view of the instrument is large ($\pm 26^\circ$), the measured particles are a combination of trapped and precipitating populations, dominated by the trapped population. Based on Polar Operational Environmental Satellite measurements, which have two detectors, one pointing zenith and the other pointing in the perpendicular direction [e.g., Rodger *et al.*, 2010], for the same time period (5–25 October 2012), the ratio of precipitating to locally mirroring electrons for $L=3\text{--}7$ is much less than 0.1.

3. Results and Discussion

[13] Figure 4 shows over the first 20 days electron fluxes in three energy channels measured by REPTile as well as the Dst index during this same time period. Several interesting features are apparent. (1) Two separate belts are visible, with the slot region in between. The inner belt electrons are only detectable when the spacecraft traverses over the South Atlantic Anomaly (SAA) region, and they are subject to contamination from the energetic protons at low L (<2), which will be further discussed in the next figure. (2) Lower energy electrons (channel 1) become enhanced first (early on 9 October) and penetrate into the slot region, some of them merging with the inner belt. Higher energy electrons (channels 2 and 3) are enhanced later, and the inner edge of these more energetic electrons moves slowly inward but never goes below $L=3$. (3) White areas of the plots indicate a lack of data coverage. Some large L regions are not covered due to

the orbit inclination and the tilt of the Earth's magnetic dipole with respect to the rotation axis. Also, the data are not acquired 100% due to occasional dropped data packets, and a spacecraft anomaly on 15 October caused a large data gap. An analog-to-digital converter is believed to have had a latch-up, draining the battery, and the spacecraft went into safe mode, shutting off the instrument. (4) The asymmetry of the magnetic field in geographic longitude creates the daily periodicity observable in the outer belt, as REPTile measures different electron populations throughout its orbit. These populations will be discussed in more detail in Figure 7.

[14] Figure 5 shows electron and proton fluxes in the first two energy channels plotted versus geographic longitude and latitude for the first 20 days of REPTile operation. The electrons are seen again in a two-belt structure, with lower energy electrons penetrating into the lower L region and some of them merging into the inner belt. There are no solar energetic particle (SEP) events during this period nor are any SEPs detected in the outer belt. Energetic protons are thus detectable only when the CubeSat is above the SAA region. It is worth noting that the intensity of 9–18 MeV protons is lower than 18–30 MeV protons, which is consistent with previous findings [Fischer *et al.*, 1977; Selesnick *et al.*, 2007], due to the faster loss of lower energy protons created by galactic cosmic ray albedo neutral decay. Except for in the center of the SAA region, where some proton contamination of the electron measurements occurs, the electrons and protons are well separated. Figures 4 and 5 demonstrate that REPTile

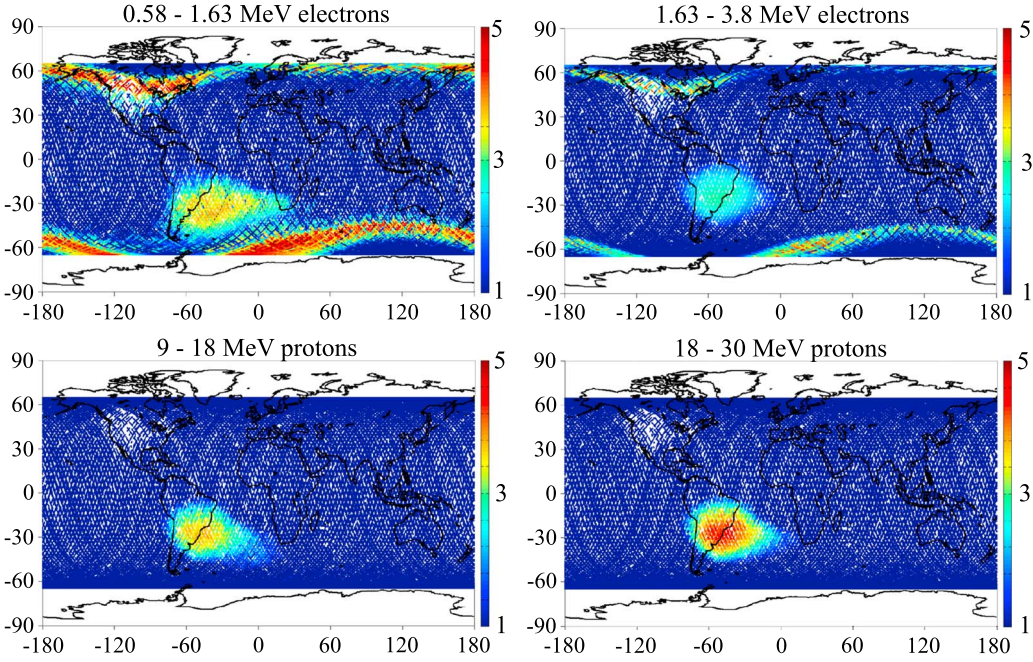


Figure 5. Mercator map of electron and proton fluxes from the first two energy channels of REPTile for the first 20 days of the mission.

measurements provide a clear picture of energetic particles (electrons and protons) in the near-Earth environment.

3.1. Comparison With Van Allen Probe Measurements

[15] Figure 6 shows a comparison of measurements between REPTile and MagEIS and also the solar wind conditions and Dst index for 5–15 October 2012. The similarity between the measurements made by REPTile, in a highly inclined LEO, and MagEIS, in a geo-transfer-like orbit, is clearly evident here (electron fluxes from our highest energy channel, >3.8 MeV, also have similar variation in comparison with REPT, not shown here). They both show the distinct two-belt structure before 9 October, and even the shape of the slot region in the top two panels looks remarkably similar. After 9 October, electrons at all energies became enhanced, but lower energy electrons were enhanced earlier and penetrated further inward. Some of the lower energy electrons merged with the inner belt, while the higher energy electrons enhanced later and did not penetrate as deep. Although higher energy electrons still slowly diffused inward, they did not go below $L = 3$. Higher energy electrons can penetrate into the slot region only during periods of stronger geomagnetic activity or solar wind conditions [Tverskaya, 1986; Zhao and Li, 2013].

[16] As pointed out by Reeves *et al.* [2003, 2013], geomagnetic storms can either intensify or deplete the fluxes of MeV electrons in the outer belt and the outer belt electron fluxes remained low and fairly constant until 8 October. Reeves *et al.* [2013] have done detailed phase space density analysis based on MagEIS and REPT and also Time History of Events and Macroscale Interactions during Substorms/Solid State Telescope (THEMIS/SST) (at larger L) measurements for the electron enhancement on and after 9 October and concluded that local acceleration is mainly responsible for the rapid enhancement of very energetic electrons ($\mu = 3433 \text{ MeV/G}$, equivalent to 2.46 MeV for an equatorially mirroring electron at $5 R_E$). However, due to the small equatorial loss cone (only a few

degrees), REPT and MagEIS are incapable of directly determining how many electrons during the enhancement are lost by precipitating into the atmosphere. That means that the actual acceleration responsible for the observed enhancement has to be more significant than what the phase space density profile indicates. REPTile, on the other hand, only measures the fraction of the total electron population that has small enough equatorial pitch angles to reach its altitude, but its measurements include the stably trapped, quasi-trapped, and precipitating (i.e., untrapped) populations. Next, we show and discuss the contribution of the precipitation loss during this 9 October storm event.

3.2. Three Populations of Outer Belt Electrons Measured by CSSWE

[17] Figure 7 shows three populations of electrons, trapped, quasi-trapped, and untrapped, that are measured by REPTile along its orbit for the first 20 days of its mission. The calculation is based on REPTile's position (altitude, latitude, and longitude) versus the local magnetic field (International Geomagnetic Reference Field (IGRF)) and assumes that electrons are locally mirroring and that an electron will be lost if it reaches 100 km altitude. As discussed earlier (Figure 3), for the vast majority of the time, REPTile's look direction is close to 90° to the local magnetic field. Based on REPTile's position at a given time, the measured electrons (assuming locally mirroring) are either (i) in the bounce loss cone (BLC), i.e., lost at its conjugate point; (ii) in the drift loss cone (DLC), i.e., lost after drifting to the SAA; or (iii) stably trapped, i.e., able to complete a drift orbit. Loss through the magnetopause is not considered here [Li *et al.*, 1997; Turner *et al.*, 2012], and the black region shows where the L value is greater than 11. Figure 8 shows the fluxes of these three populations of electrons measured by REPTile. It is clear that only a very small fraction is in the BLC (lost within one bounce motion, less than a second), the majority of the measurements is in the DLC (lost within one drift period: $\sim 10 \text{ min}$, depending on

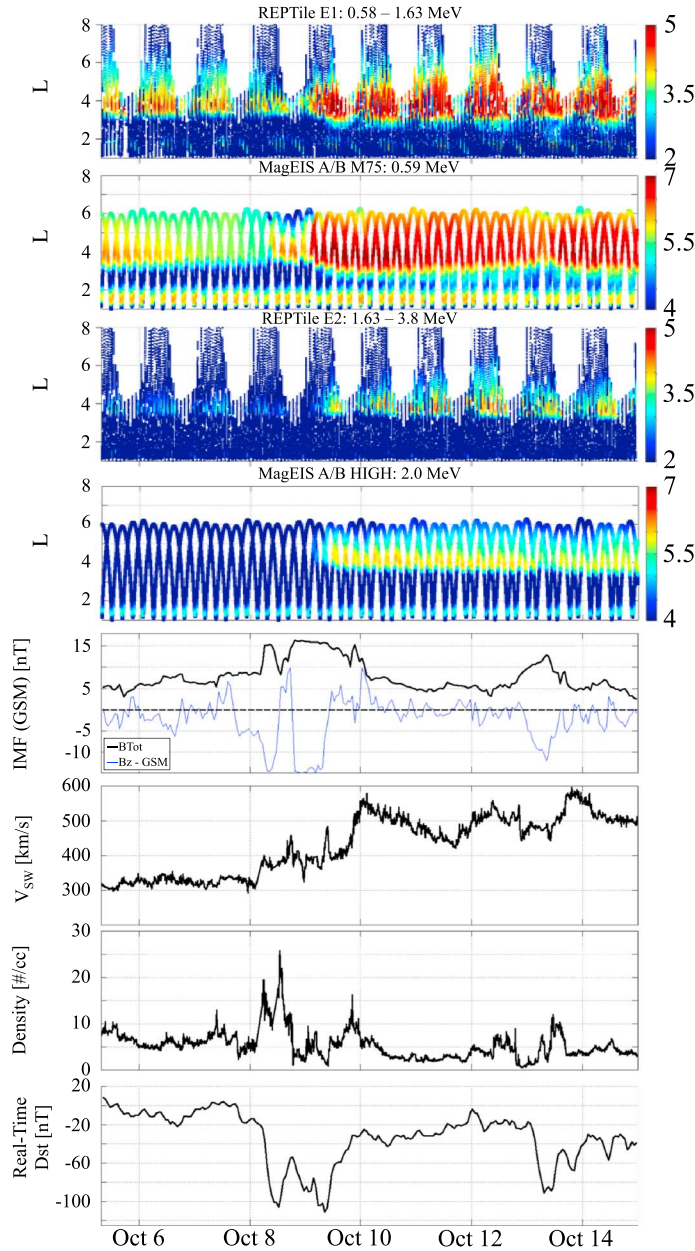


Figure 6. Comparison between measurements made by REPTile and MagEIS, as well as solar wind conditions (from ACE) and the Dst index. Top four panels show color coded in logarithm and sorted in L (L bin: 0.1) electron fluxes from REPTile (every 6 s) and MagEIS (spin-averaged data, spin period: 10 s) for the indicated energy range.

the energy and L value) and trapped (continuing to drift around). Based on the ratio between the quasi-trapped electron content and the total electron content, we can estimate the loss rate of the electrons.

3.3. Estimation of the Electron Loss Rate From REPTile Data

[18] Based on the data analysis described in the previous section, we can estimate the electron loss rate from REPTile data alone, using a simple calculation of the relative stably trapped and quasi-trapped intensity levels identified from the measured electrons. Since the low-altitude electron distribution is a balance between azimuthal drift and pitch

angle diffusion, a drift-diffusion model was developed to simulate the low-altitude electron distribution observed by SAMPEX (in a similar orbit as CSSWE) and obtained estimates of the associated loss rates [Selesnick, 2006; Tu *et al.*, 2010]. Considering that electrons in the DLC must drift into the SAA region and be lost from the radiation belt within one drift period, τ_d , the DLC content should be related to the mean electron lifetime assuming that this content is steadily being replenished by pitch angle diffusion. Based on numerical model solutions from the drift-diffusion model in Selesnick [2006], the electron lifetime, τ , can be estimated as $\tau_d/7F$ over a broad range of diffusion coefficients (typo correction of the original equation, $7\tau_d/F$, has been made

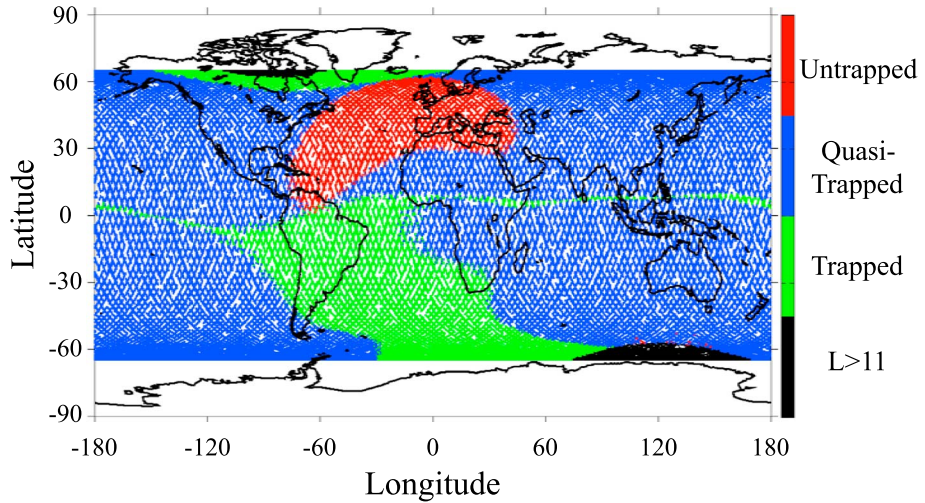


Figure 7. The trapped, quasi-trapped (within drift loss cone), untrapped (within bounce loss cone) electron populations, based on REPTile's position and the IGRF magnetic field model, are shown in blue, green, and red, respectively, assuming the measured electrons are locally mirroring and the electron will be lost when it reaches or goes below 100 km altitude. The black region shows where the L value is greater than 11.

after discussion with Dr. Selesnick), where F is the ratio of the quasi-trapped population to the total, locally measured population averaged over half a day. This is called the Loss Index Method. The assumption for this method breaks down when the diffusion rate increases to the point where the DLC

is nearly full (nearly isotropic flux distribution between trapped and DLC electrons), so that the fraction F cannot increase with further diffusion rate increases [Selesnick, 2006]. This occurs when $F \geq 0.02$, in which case the estimated lifetime only provides an upper limit for the real lifetime.

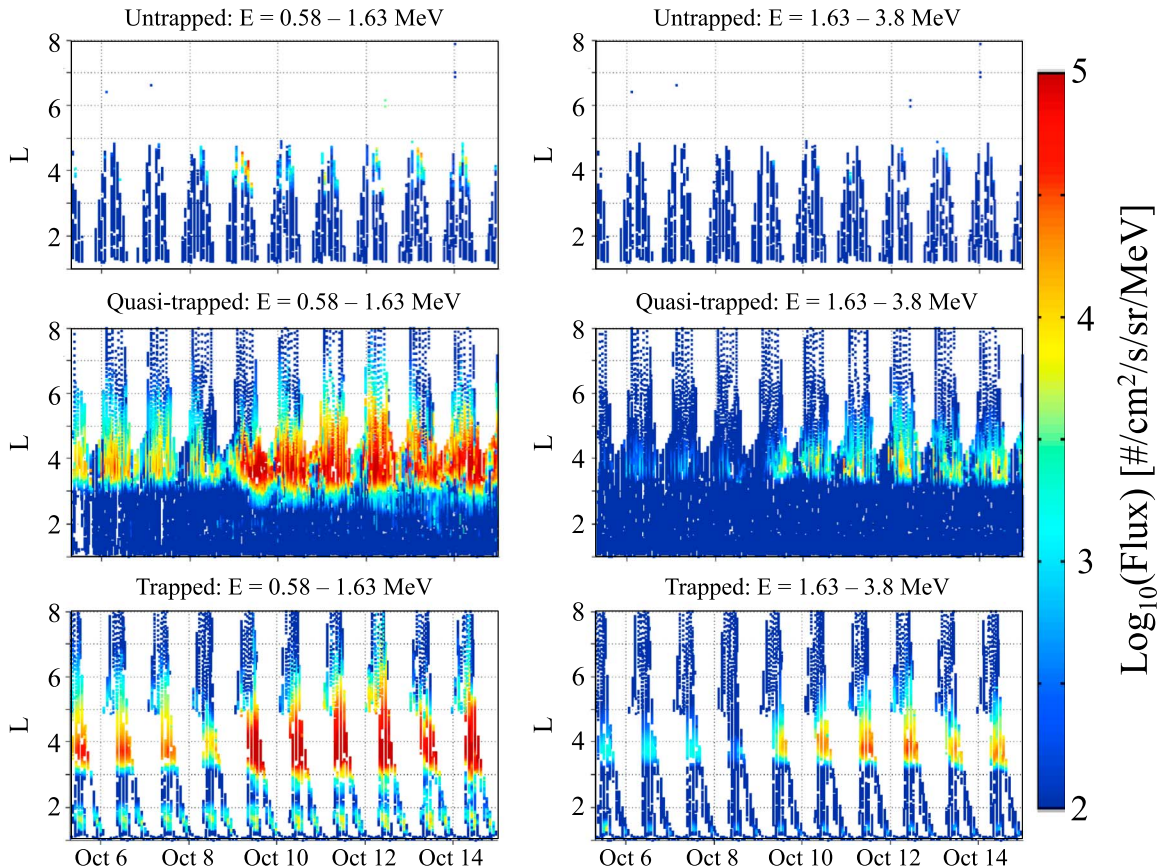


Figure 8. Fluxes of the three populations of the electrons measured by REPTile in its first two energy channels, color coded in logarithm and sorted in L (L bin: 0.1) for the first 10 days of operation.

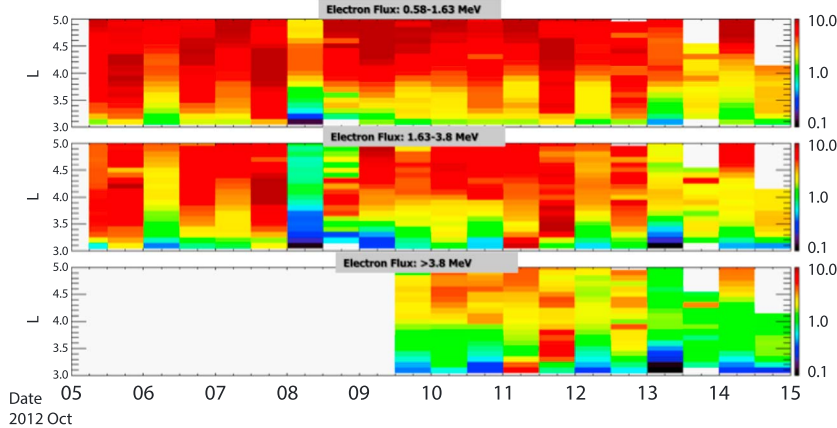


Figure 9. The lifetime for the electrons, τ (color bar in days), measured by REPTile for the first 10 days, estimated based on the ratio between quasi-trapped and trapped populations using the Loss Index Method, which is discussed in the text.

Using the Loss Index Method, we calculate the electron lifetime at $L=3\text{--}5$ for the October 2012 storm and show the results in Figure 9 for three energy channels from REPTile. During the first half of 9 October, F is calculated to be less than 0.02 around $L=4$, thus the Loss Index Method is applicable.

[19] With near-equatorial measurements using REPT and MagEIS data, Reeves *et al.* [2013] examined this same event and found that there was a rapid (~ 12 h), 3 orders of magnitude enhancement of relativistic electrons centered around $L \sim 4$ (i.e., near the location of the growing phase space density peak). However, from the CSSWE observations with REPTile, we know that there was also some loss to the atmosphere throughout the outer belt during this period. So, accounting for the competition between electron acceleration and loss processes, the enhancement observed by Van Allen

Probes must actually have been stronger than what was observed by the two equatorial spacecraft. Based on our analysis using the Loss Index Method, the estimated losses reveal that the total enhancements during the 9 October 2012 storm were actually at least 12.7% stronger for 0.58 MeV electrons and 14.6% stronger for 1.63 MeV electrons around $L=4$ than the observed enhancements from the Van Allen Probes observations shown in Reeves *et al.* [2013].

[20] Finally, Figure 10 shows daily averaged electron fluxes from the lower two energy channels of REPTile for the first ~ 6 months of the mission, demonstrating the dynamic features of the outer belt electrons, including the slow decay starting at the middle of December of 2012, during which the Dst never went below -25 nT for over 20 days, and the sudden enhancement of 0.58–1.63 MeV electrons near 13 January 2013 while there was not a

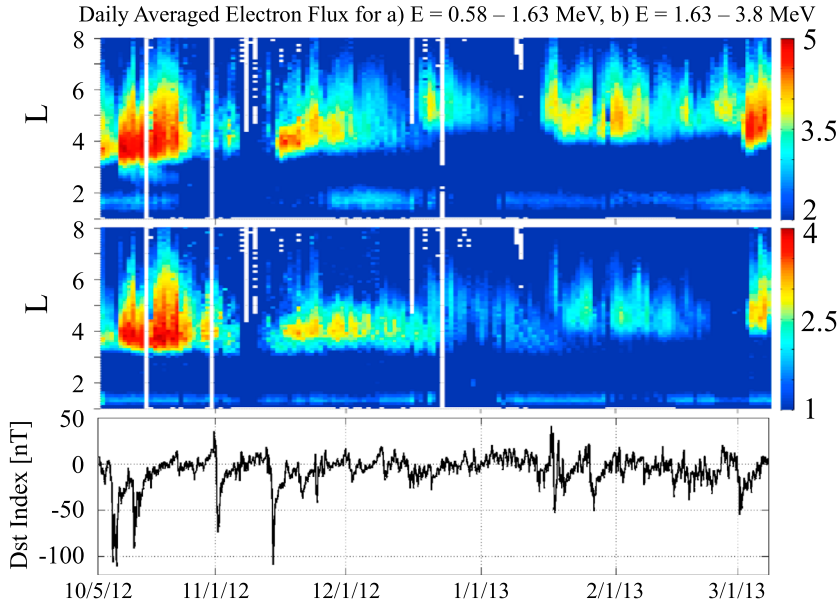


Figure 10. Daily averaged electron fluxes from the lower two energy channels of REPTile and the Dst index for the first ~ 6 months of the mission. Several data gaps are due to anomalies that sent the spacecraft into the safe mode. The instrument did not operate at 100% duty cycle during some periods, leading to some irregularity, such as the on-and-off inner belt appearance.

magnetic storm (Dst was above -25 nT). Many such interesting events are under investigation and will be discussed in detail in future publications.

4. Summary and Conclusions

[21] Here we have shown the first science results from the CSSWE CubeSat mission, using data from its sole science instrument, REPTile. From CSSWE's highly inclined LEO, REPTile measures relativistic electrons ranging from 0.58 to >3.8 MeV and protons from 9 to 40 MeV. Furthermore, like SAMPEX, REPTile data can be used to distinguish between trapped, quasi-trapped, and precipitating (i.e., untrapped) particles based on its location and orientation with respect to the local magnetic field. Great care has been taken to properly process and clean the raw count rates from REPTile to produce reliable differential fluxes of energetic particles, and we have also presented details of the conversion process here. From the first 6 months of processed flux data, we have shown that REPTile observations clearly measured the distinct inner and outer radiation belt electron populations, showed previously understood characteristics of the inner zone protons such as the shorter lifetimes at lower energies, and were consistent with Van Allen Probes observations of outer electron belt variations. In short, these REPTile data demonstrate that high-quality scientific measurements are obtainable from student-led and developed CubeSat missions.

[22] We have examined the early October 2012 storms in detail. Using REPTile observations of relativistic electrons from LEO, we quantify the percent loss of electrons scattered into the atmospheric loss cones during the rapid enhancement of the outer belt around $L \sim 4$ on 9 October 2012. These results are compared to the equatorial observations from the MagEIS instrument on NASA's Van Allen Probes spacecraft. Our results indicate that the enhancement during this period was actually at least 12.7% and 14.6% stronger for 0.58 and 1.63 MeV electrons, respectively, at $L \sim 4$, compared to that observed by the Van Allen Probes at high altitude. These results demonstrate the significance of competing loss processes, in particular loss due to atmospheric precipitation, during acceleration events and the critical importance of LEO observations for quantifying precipitation losses and better understanding variations of relativistic outer belt electrons. The results also suggest possible energy dependencies of the competing source and loss processes [e.g., Bortnik and Thorne, 2007; Thorne et al., 2013] during this event, which should be of interest for future studies.

[23] From the results presented here, CSSWE is a prime example of how CubeSats can be used to complement larger missions by providing additional data points and types of measurements that are not possible with the larger mission alone. This demonstrates how, with strategic deployment during future and/or ongoing missions, small and inexpensive CubeSats can significantly enhance the science return of larger missions.

[24] **Acknowledgments.** We would like to thank Richard Selesnick and Mike Temerin for their helpful discussions. This work is mainly supported by NSF (CubeSat program) grant AGSW 0940277 and also NASA contract NASS-01072 (Van Allen Probes mission) and NASS-02099 (THEMIS mission).

[25] Robert Lysak thanks Ioannis Daglis and James McCollough for their assistance in evaluating this paper.

References

- Agostinelli, S., et al. (2003), Nuclear instruments and methods in physics research section A: accelerators, spectrometers, detectors and associated equipment, *Nucl. Instrum. Methods A*, **506**, 250–303.
- Baker, D. N., P. R. Higbie, R. D. Belian, and E. W. Hones Jr. (1979), Do Jovian electrons influence the terrestrial outer radiation zone?, *Geophys. Res. Lett.*, **6**(6), 531–534.
- Baker, D. N., et al. (1998), A strong CME-related magnetic cloud interaction with the Earth's magnetosphere: ISTP observation of rapid relativistic electron acceleration on May 15, 1997, *Geophys. Res. Lett.*, **25**, 2975–2978.
- Baker, D. N., S. G. Kanekal, T. I. Pulkkinen, and J. B. Blake (1999), Equinoctial and solstitial averages of magnetospheric relativistic electrons: A strong semiannual modulation, *Geophys. Res. Lett.*, **26**, 3193–3196.
- Baker, D. N., et al. (2012), The relativistic electron-proton telescope (REPT) instrument on board the radiation belt storm probes (RBSP) spacecraft: Characterization of Earth's radiation belt high-energy particle populations, *Space Sci. Rev.*, doi:10.1007/s11214-012-9950-9.
- Barker, A. B., X. Li, and R. S. Selesnick (2005), Modeling the radiation belt electrons with radial diffusion driven by the solar wind, *Space Weather*, **3**, S10003, doi:10.1029/2004SW000118.
- Blake, J. B., et al. (2013), The magnetic electron ion spectrometer (MagEIS) instruments aboard the radiation belt storm probes (RBSP) spacecraft, *Space Sci. Rev.*, doi:10.1007/s11214-013-9991-8.
- Bortnik, J., and R. M. Thorne (2007), The dual role of ELF/VLF chorus waves in the acceleration and precipitation of radiation belt electrons, *J. Atmos. Sol. Terr. Phys.*, **69**, 378–386.
- Burton, R., S. Rock, J. Springmann, and J. Cutler (2013), Online attitude determination of a passively magnetically stabilized spacecraft, *Proceedings of the 23rd AAS/AIAA Space Flight Mechanics Meeting*, pp 1–18.
- Chen, Y., G. D. Reeves, and R. H. W. Friedel (2007), The energization of relativistic electrons in the outer Van Allen radiation belt, *Nat. Phys.*, **3**, 614–617, doi:10.1038/nphys655.
- Cook, W. R., et al. (1993), PET: A proton/electron telescope for studies of magnetospheric, solar, and galactic particles, *IEEE Trans. Geosci. Remote Sens.*, **31**, 565–571.
- Elkington, S. R., M. K. Hudson, and A. A. Chan (1999), Acceleration of relativistic electrons via drift-resonant interaction with toroidal-mode Pe-5 ULF oscillations, *Geophys. Res. Lett.*, **26**, 3273.
- Engelbreton, M., K.-H. Glassmeier, M. Stellmacher, W. J. Hughes, and H. Lühr (1998), The dependence of high-latitude Pe5 wave power on solar wind velocity and on the phase of high-speed solar wind streams, *J. Geophys. Res.*, **103**, 26,271.
- Fischer, H. M., V. W. Auschrat, and G. Wibberenz (1977), Angular distribution and energy spectra of protons of energy $5 \leq E \leq 50$ MeV at the lower edge of the radiation belt in equatorial latitudes, *J. Geophys. Res.*, **82**(4), 537–547, doi:10.1029/JA082i004p00537.
- Horne, R. B., and R. M. Thorne (2003), Relativistic electron acceleration and precipitation during resonant interactions with whistler-mode chorus, *Geophys. Res. Lett.*, **30**(10), 1527, doi:10.1029/2003GL016973.
- Hudson, M. K., S. R. Elkington, J. G. Lyon, C. C. Goodrich, and T. J. Rosenberg (1999), Simulation of radiation belt dynamics driven by solar wind variations, in *Sun-Earth Plasma Connections*, *Geophys. Monogr. Ser.*, vol. 109, edited by L. Burch, L. Carovillano, and K. Antiochos, pp. 171–182, AGU, Washington, D. C., doi:10.1029/GM109p0171.
- Kasahara, Y., Y. Miyoshi, Y. Omura, O. P. Verkhoglyadova, I. Nagano, I. Kimura, and B. T. Tsurutani (2009), Simultaneous satellite observations of VLF chorus, hot and relativistic electrons in a magnetic storm “recovery” phase, *Geophys. Res. Lett.*, **36**, L01106, doi:10.1029/2008GL036454.
- Kessel, R. L., N. J. Fox, and M. Weiss (2012), The radiation belt storm probes (RBSP) and space weather, *Space Sci. Rev.*, doi:10.1007/s11214-012-9953-6.
- Kress, B. T., M. K. Hudson, M. D. Looper, J. Albert, J. G. Lyon, and C. C. Goodrich (2007), Global MHD test particle simulations of solar energetic electron trapping in the Earth's radiation belts, *J. Atmos. Sol. Terr. Phys.*, **70**, 1727.
- Li, X., D. N. Baker, M. Temerin, T. E. Cayton, E. Reeves, R. A. Christensen, J. B. Blake, M. D. Looper, R. Nakamura, and S. G. Kanekal (1997), Multisatellite observations of the outer zone electron variation during the November 3–4, 1993, magnetic storm, *J. Geophys. Res.*, **102**(A7), 14,123–14,140.
- Li, X., D. N. Baker, M. Temerin, T. Cayton, G. Reeves, R. Selesnick, J. B. Blake, G. Lu, S. Kanekal, and H. Singer (1999), Rapid enhancements of relativistic electrons deep in the magnetosphere during the May 15, 1997 magnetic storm, *J. Geophys. Res.*, **104**, 4467.
- Li, X., D. N. Baker, S. G. Kanekal, M. Looper, and M. Temerin (2001), SAMPEX long term observations of MeV electrons, *Geophys. Res. Lett.*, **28**, 3827.

- Li, W., Y. Y. Shprits, and R. M. Thorne (2007), Dynamic evolution of energetic outer zone electrons due to wave-particle interactions during storms, *J. Geophys. Res.*, **112**, A10220, doi:10.1029/2007JA012368.
- Li, X., M. Temerin, D. N. Baker, and G. D. Reeves (2011a), Behavior of MeV electrons at geosynchronous orbit during last two solar cycles, *J. Geophys. Res.*, **116**, A11207, doi:10.1029/2011JA016934.
- Li, X., S. Palo, and R. Kohnert (2011b), Small space weather research mission designed fully by students, *Space Weather*, **9**, S04006, doi:10.1029/2011SW000668.
- Li, X., S. Palo, R. Kohnert, D. Gerhardt, L. Blum, Q. Schiller, D. Turner, W. Tu, N. Sheiko, and C. S. Cooper (2012), Colorado student space weather experiment: Differential flux measurements of energetic particles in a highly inclined low Earth orbit, in *Dynamics of the Earth's Radiation Belts and Inner Magnetosphere*, Geophys. Monogr. Ser., vol. 199, edited by D. Summers et al., pp. 385–404, AGU, Washington, D. C., doi:10.1029/2012GM001313.
- Li, X., S. Palo, R. Kohnert, L. Blum, D. Gerhardt, Q. Schiller, and S. Califff (2013), Small mission accomplished by students - impact on space weather research, *Space Weather*, **11**, 55–56, doi:10.1002/swe.20025.
- Markley, F. L. (2003), Attitude error representations for Kalman filtering, *J. Guid. Control. Dyn.*, **26**(2), 311–317.
- Mathie, R. A., and I. R. Mann (2000), A correlation between extended intervals of ULF wave power and storm-time geosynchronous relativistic electron flux enhancements, *Geophys. Res. Lett.*, **27**, 3261.
- Mathie, R. A., and I. R. Mann (2001), On the solar wind control of Pc5 ULF pulsation power at mid-latitudes: Implications for MeV electron acceleration in the outer radiation belt, *J. Geophys. Res.*, **106**, 29,783.
- O'Brien, T. P., and M. B. Moldwin (2003), Empirical plasmapause models from magnetic indices, *Geophys. Res. Lett.*, **30**(4), 1152, doi:10.1029/2002GL016007.
- Paulikas, G. A., and J. B. Blake (1979), Effects of the solar wind on magnetospheric dynamics: Energetic electrons at the synchronous orbit, in *Quantitative Modeling of Magnetospheric Processes*, Geophys. Monogr. Ser., vol. 21, edited by D. Summers and W. P. Olson, pp. 180–202, AGU, Washington, D. C.
- Reeves, G. D., K. L. McAdams, R. H. W. Friedel, and T. P. O'Brien (2003), Acceleration and loss of relativistic electrons during geomagnetic storms, *Geophys. Res. Lett.*, **30**(10), 1529, doi:10.1029/2002GL016513.
- Reeves, G. D., et al. (2013), Electron acceleration in the heart of the Van Allen radiation belts, *Science*, **341**(6149), 991–994, doi:10.1126/science.1237743.
- Rodger, C. J., M. A. Clilverd, J. C. Green, and M. M. Lam (2010), Use of POES SEM-2 observations to examine radiation belt dynamics and energetic electron precipitation into the atmosphere, *J. Geophys. Res.*, **115**, A04202, doi:10.1029/2008JA014023.
- Rostoker, G., S. Skone, and D. N. Baker (1998), On the origin of relativistic electrons in the magnetosphere associated with some geomagnetic storms, *Geophys. Res. Lett.*, **25**, 3701.
- Selesnick, R. S. (2006), Source and loss rates of radiation belt relativistic electrons during magnetic storms, *J. Geophys. Res.*, **111**, A04210, doi:10.1029/2005JA011473.
- Selesnick, R. S., M. D. Looper, and R. A. Mewaldt (2007), A theoretical model of the inner proton radiation belt, *Space Weather*, **5**, S04003, doi:10.1029/2006SW000275.
- Shprits, Y. Y., R. M. Thorne, R. B. Horne, S. A. Glauert, M. Cartwright, C. T. Russell, D. N. Baker, and S. G. Kanekal (2006), Acceleration mechanism responsible for the formation of the new radiation belt during the 2003 Halloween solar storm, *Geophys. Res. Lett.*, **33**, L05104, doi:10.1029/2005GL024256.
- Spence, H. E., et al. (2013), Science goals and overview of the energetic particle, composition, and thermal plasma (ECT) suite on NASA's radiation belt storm probes (RBSP) mission, *Space Sci. Rev.*, doi:10.1007/s11214-013-0007-5.
- Thorne, R. M., et al. (2013), Evolution and slow decay of an unusual narrow ring of relativistic electrons near $L \sim 3.2$ following the September 2012 magnetic storm, *Geophys. Res. Lett.*, **40**, doi:10.1002/grl.50627.
- Tu, W., and X. Li (2011), Adiabatic effects on radiation belt electrons at low altitude, *J. Geophys. Res.*, **116**, A09201, doi:10.1029/2011JA016468.
- Tu, W., X. Li, Y. Chen, G. D. Reeves, and M. Temerin (2009), Storm dependent radiation belt electron dynamics, *J. Geophys. Res.*, **114**, A02217, doi:10.1029/2008JA013480.
- Tu, W., R. Selesnick, X. Li, and M. Looper (2010), Quantification of the precipitation loss of radiation belt electrons, *J. Geophys. Res.*, **115**, A07210, doi:10.1029/2009JA014949.
- Tu, W., S. R. Elkington, X. Li, W. Liu, and J. Bonnell (2012), Quantifying radial diffusion coefficients of radiation belt electrons based on global MHD simulation and spacecraft measurements, *J. Geophys. Res.*, **117**, A10210, doi:10.1029/2012JA017901.
- Turner, D. L., Y. Shprits, M. Hartinger, and V. Angelopoulos (2012), Explaining sudden losses of outer radiation belt electrons during geomagnetic storms, *Nat. Phys.*, **8**, 208–212, doi:10.1038/nphys2185.
- Turner, D. L., V. Angelopoulos, W. Li, M. D. Hartinger, M. Usanova, I. R. Mann, J. Bortnik, and Y. Shprits (2013), On the storm-time evolution of relativistic electron phase space density in Earth's outer radiation belt, *J. Geophys. Res. Space Physics*, **118**, 2196–2212, doi:10.1002/jgra.50151.
- Tverskaya, L. V. (1986), On the boundary of electron injection into the magnetosphere, *Geomag. Aeron.*, **26**(5), 864–865.
- Ukhorskiy, A. Y., B. J. Anderson, K. Takahashi, and N. A. Tsyganenko (2006), The impact of ULF oscillations in solar wind dynamic pressure on the outer radiation belt electrons, *Geophys. Res. Lett.*, **33**, L06111, doi:10.1029/2005GL024380.
- Van Allen, J. A., D. N. Baker, B. A. Randall, and D. D. Sentman (1974), The magnetosphere of Jupiter as observed with Pioneer 10: 1. Instrument and principal findings, *J. Geophys. Res.*, **79**(25), 3559–3577.
- Vennstrom, S. (1999), Dayside magnetic ULF power at high latitudes: A possible long-term proxy for the solar wind velocity?, *J. Geophys. Res.*, **104**, 10,145.
- Williams, D. J. (1966), A 27-day periodicity in outer zone trapped electron intensities, *J. Geophys. Res.*, **71**, 1815.
- Yoon, P. H. (2011), Large-amplitude whistler waves and electron acceleration, *Geophys. Res. Lett.*, **38**, L12105, doi:10.1029/2011GL047893.
- Zhao, H., and X. Li (2013), Inward shift of outer radiation belt electrons as a function of Dst index and the influence of the solar wind on electron injections into the slot region, *J. Geophys. Res. Space Physics*, **118**, 1–9, doi:10.1029/2012JA018179.